p53 controls the nuclear entry and epigenetic modification of H3.1 by downregulating nuclear phosphatidic acid

Tsukasa Oikawa,[1]* Junya Hasegawa,[2] Naomi Ohnishi,[3] Yasuhito Onodera,[1,4] Ari Hashimoto,[1] Junko Sasaki, [2] Takehiko Sasaki,[2] Koji Ueda,[3] and Hisataka Sabe[1,5]*

[1]Department of Molecular Biology, Graduate School of Medicine, Hokkaido University, North 15, West 7, Kita-ku, Sapporo, Hokkaido 060-8638, Japan

[2]Department of Biochemical Pathophysiology/Lipid Biology, Medical Research Institute, Tokyo Medical and Dental University, 1-5-45 Yushima, Bunkyo-ku, Tokyo 113-8510, Japan

[3]Cancer Proteomics Group, Cancer Precision Medicine Center, Japanese Foundation for Cancer Research, 3-8-31 Ariake, Koto-ku, Tokyo 135-8550, Japan

[4]Global Center for Biomedical Science and Engineering, Graduate School of Medicine, Hokkaido University, North 15, West 7, Kita-ku, Sapporo, Hokkaido 060-8638, Japan

[5]Institute for Genetic Medicine, Hokkaido University, North 15, West 7, Kita-ku, Sapporo, Hokkaido 060-8638, Japan

*To whom correspondence should be addressed

E-mail: oikawa_tsukasa@med.hokudai.ac.jp; sabeh@med.hokudai.ac.jp

Tel.: +81-11-706-5045; Fax: +81-11-706-7865

Key words: H3.1; p53; CTDNEP1; EZH2; H3K27me3; Phosphatidic acid; DNA replication; Nuclear lamina

Abstract

H3.1 is predominantly synthesized and enters the nucleus during the G1/S phase of the cell cycle, although the underlying mechanism remains unknown. Here we show that p53 is involved in this process. CTDNEP1 converts phosphatidic acid (PA) into diacylglycerol, and EZH2 generates H3K27me3. p53 increased CTDNEP1 and decreased EZH2 in the nuclear H3.1 interactome of the G1/S phase. Moreover, H3.1 bound robustly to PA but not to diacylglycerol. p53 deficiency caused perinuclear accumulation of EZH2-modified H3K27me3 of non-nucleosomal histones during the G1/S phase. p53 induced the expression of *TMEM255A*, which reduced nuclear PA levels by increasing CTDNEP1 levels. Therefore, H3.1 entering the nucleus in the absence of p53 may be trapped near the nuclear envelope (NE) and epigenetically marked as repressive without forming nucleosomes. Our study identified the NE as a novel target of p53, in which p53 downregulates nuclear PA levels to normalize H3.1 nuclear entry and epigenetic modification.

Introduction

Molecular processes involved in the nuclear transport and usage of histones in the nucleus are thought to be closely associated with genome regulation and integrity. For example, molecular chaperones and transporters involved in the nuclear transport of H3-histones have been extensively studied [1-9]. H3.1 is an S phase-specific histone, which is predominantly synthesized in and enters the nucleus during the S phase of the cell cycle [10]. Upon entry into the nucleus, H3.1 has been shown to be complexed with chromatin assembly factor 1 and guided to sites of DNA replication [11, 12]. On the other hand, processes associated with the nuclear entry of histones remain largely unknown.

To analyze the mechanism of nuclear entry of histones, we here focused on H3.1, because the nuclear entry of this histone is specific to the G1/S phase, and hence its analysis was expected to be simpler than that of other histones. The lipid content of the nuclear envelope (NE) is dynamically and locally remodeled during cell cycle progression [13, 14]. We found that p53, a product of the tumor suppressor gene *TP53*, is required for H3.1 to properly enter the nucleus, in which p53 plays a role in modulating the composition of certain lipids in the nucleus. This function of p53 appears to be partly mediated by the induction of a p53-target gene, *TMEM255A*, and the protein product of this gene then acts to increase levels of a lipid phosphatase in the nucleus. On the other hand, if H3.1 molecules enter the nucleus in the absence of p53, they may be at least transiently accumulated in the vicinity of the NE, owing to the loss of p53-mediated modulation of nuclear lipid composition, and are likely to be

epigenetically marked as repressive before interacting with DNA and before forming nucleosomes. Our results provide molecular insights into a novel function of p53, in which p53 modulates nuclear lipid compositions to ensure the proper nuclear entry of H3.1 as well as its proper epigenetic modification, and hence normalize H3.1 usage in the nucleus.

Results

Loss of p53 causes the perinuclear accumulation of lysine 27-trimethylated histone H3 (H3K27me3)

Using super-resolution three-dimensional structured illumination microscopy (SIM), we found that silencing of *TP53* by siRNAs (si*TP53*) in normal human mammary epithelial HMLE cells causes the accumulation of H3K27me3, but not lysine 4-trimethylated histone H3 (H3K4me3) or lysine 27-acetylated histone H3 (H3K27ac), near the NE (Fig. 1, A, B, and C). H3K27me3, H3K4me3, and H3K27ac were spread throughout the nucleus in control cells (*i.e.*, si*Scr* cells) (Fig. 1A). si*TP53* treatment of the human cancer cell lines A549 and MCF7 also caused similar perinuclear accumulation of H3K27me3 (Fig. 1C and S1A). Levels of these histone modifications were not notably affected by si*TP53* (Fig. 1D). Similar accumulation of H3K27me3 was also observed in the human cancer cell line H1299, which lacks p53 expression, and in the mouse embryonic fibroblast cell line MB352 established from *Trp53*$^{-/-}$ mice (Fig. 1E). Therefore, p53 deficiency may cause the aberrant perinuclear accumulation of H3K27me3 in different types of cells, including cancer cells, and in humans and mice.

Perinuclear accumulation of H3K27me3 occurs during the G1/S phase

We then investigated whether H3K27me3 accumulation occurs during a specific phase of the cell cycle. H1299 cells and MB352 cells stably expressing the cell cycle indicator Fucci [15] demonstrated that H3K27me3 accumulation occurs predominantly from the late G1 to the early S phase in the absence of p53 (Fig. 1F). Thymidine-blockade of G1/S

progression in H1299 cells also caused H3K27me3 accumulation (Fig. 1G). Therefore, the perinuclear accumulation of H3K27me3 in the absence of p53 appeared to occur predominantly during the G1/S phase.

p53 suppresses H3K27me3 accumulation without cell-cycle arrest or apoptosis

Expression of wild-type p53 (p53 WT) significantly decreased H3K27me3 accumulation in thymidine-blocked H1299 cells and MB352 cells (Fig. 1G). However, p53 may induce genes involved in cell-cycle arrest or apoptosis [16] (Fig. 1H, Fig. S1C). We then used a p53 mutant, p53 QM, bearing the L22Q/W23S/W53Q/F54S mutations, which was previously shown to not induce expression of such genes (see Fig. S1B) [17]. We here confirmed that p53 QM did not induce genes known to be involved in cell-cycle arrest, apoptosis, and metabolism, when expressed in H1299 cells and MB352 cells (Fig. 1H, Fig. S1, B and C, Fig. S2, and Table S1). Nevertheless, p53 QM substantially suppressed the accumulation of H3K27me3 in these cells (Fig. 1, G and I). Furthermore, the proximity ligation assay (PLA) coupled with SIM imaging in thymidine-blocked H1299 cells demonstrated that the expression of p53 QM significantly reduces the colocalization of H3K27me3 with lamin A/C near the NE (Fig. 1, J and K). Therefore, p53 appears to suppress the aberrant perinuclear accumulation of H3K27me3 and its colocalization with lamin A/C during the G1/S phase, likely independent of cell-cycle arrest, apoptosis, and metabolic remodeling.

Properties of perinuclearly accumulated H3K27me3 histones

We then investigated the properties of the perinuclearly accumulated H3K27me3 histones. Costaining of H3K27me3 with lamin A/C in H1299 cells showed their close colocalization with the NE (Fig. 2A). Their costaining with DNA then suggested that these histones are not well colocalized with DNA (Fig. 2B). We then visualized the DNA replication sites using biotin-labeled deoxyuridine triphosphate (dUTP) [18, 19]. SIM imaging of H1299 cells, blocked once with thymidine and then released for 20 min, revealed that most of the perinuclearly accumulated H3K27me3 histones were not localized to DNA replication sites, whereas the localization of H3K27me3 histones to DNA replication sites was clearly detected in the presence of p53 QM (Fig. 2, C and D).

We furthermore analyzed the possible nucleosome formation of these histones. PLA between H3K27me3 and H4 in the thymidine-blocked H1299 cells demonstrated that most of the PLA signals were found inside the nucleoplasm rather than near the NE (Fig. 2, E and F). Furthermore, levels of these signals near the NE were not notably changed irrespective of p53 QM (Fig. 2, E and F). Thus, most of the H3K27me3 histones accumulated near the NE in the absence of p53 did not appear to have formed nucleosomes, bound to DNA, or localized to DNA replication sites.

H3.1/H3.2 comprises the accumulated H3K27me3

H3.1 and H3.2 are synthesized in the cytosol and then transported into the nucleus during the G1/S phase of the cell cycle, whereas H3.3 acts independently of DNA replication [10, 11]. These H3 variants were expressed at similar levels in H1299 cells

irrespective of p53 QM expression or thymidine blockade (Fig. 3A). Using antibodies specific to H3.1/H3.2 and to H3.3, we then found that H3.1/H3.2, but not H3.3, accumulated near the NE in the thymidine-blocked H1299 cells (Fig. 3B), and that such accumulation was largely mitigated by p53 QM (Fig. 3C). Thus, H3.1/H3.2, but not H3.3, appear to predominantly comprise the perinuclearly accumulated H3K27me3 histones. Antibodies that selectively recognize either H3.1 or H3.2 were not available, and it hence remains unclear as to which of them comprise the accumulated H3K27me3 histones.

p53 increases CTDNEP1 and decreases EZH2 levels in the nuclear H3.1 interactome

We then sought to obtain a clue to link p53 with H3.1/H3.2. For this purpose, we performed an interactome analysis using liquid chromatography-mass spectrometry on anti-H3 immunoprecipitants from the nuclear fraction of thymidine-blocked H1299 cells (Fig. 3D). Proteins were crosslinked with dithiobis(succinimidyl propionate) (DSP) before solubilization. Notably, we found that the anti-H3 antibody predominantly pulled down H3.1 under this condition, rather than H3.2 or H3.3 (Fig. 3E and Table S2), although we do not have a clear explanation for this. Among the different proteins that were coprecipitated, the amount of C-terminal domain nuclear envelope phosphatase 1 (CTDNEP1) was more than 4-fold higher in the presence of p53 QM than in its absence (Fig. 3E and Table S2). Enhancer of zeste homolog 2 (EZH2) was also coprecipitated, but its amount was about 2-fold lower in the presence of p53 than in its absence (Fig.

3E and Table S2). The amounts of H3.1 in immunoprecipitants were not notably changed irrespective of the presence/absence of p53 QM, and p53 was coprecipitated when present (Fig. 3E and Table S2). Thus, p53 may play a role in increasing CTDNEP1 and decreasing EZH2 levels in the nuclear H3.1 interactome formed during the G1/S phase.

p53 suppresses the perinuclear interaction of H3.1 with EZH2

We then focused on EZH2. EZH2 is a catalytic subunit of Polycomb Repressive Complex 2, which generates H3K27me3 [20]. We confirmed the above results by western blotting, in which a larger amount of EZH2 was detected in anti-H3 immunoprecipitants from the G1/S-arrested cells in the absence of p53 QM (Fig. 4A). Benzonase is a potent endonuclease, and benzonase treatment during immunoprecipitation did not affect the amounts of the coprecipitated EZH2, avoiding the possible contamination of nuclear DNA (Fig. 4A).

si*EZH2* substantially mitigated the perinuclear accumulation of H3K27me3 in these thymidine-blocked H1299 cells (Fig. 4B). Western blot analysis showed that si*EZH2* reduced the total cellular amounts of H3K27me3, but not H3K4me3 (Fig. 4C). In addition, the PLA assay showed that p53 QM significantly suppresses the colocalization between EZH2 and H3 near the NE in the G1/S-arrested cells (Fig. 4, D and E). Taken together, therefore, it is likely that EZH2 is responsible for the generation of the perinuclearly accumulated H3K27me3, whereas p53 may act to suppress the

perinuclear interaction between H3 and EZH2. As H3.1/H3.2 appeared to predominantly comprise the accumulated H3K27me3-histones, these aberrantly accumulated histones are likely to be those newly entering the nucleus during the G1/S phase.

p53 uses CTDNEP1 to reduce the level of nuclear phosphatidic acid

We next focused on CTDNEP1, which was increased in the H3.1 interactome by p53. CTDNEP1 converts phosphatidic acid (PA) to diacylglycerol (DAG) via activating the Lipin PA phosphatases [14, 21-23]. PA is a major precursor of other lipids [14]. We found that H3.1 demonstrates a robust affinity to PA, but not to DAG (Fig. 5A). We hence tested whether CTDNEP1 plays a role in reducing nuclear PA levels, as well as in reducing the perinuclear accumulation of H3K27me3. We performed mass spectrometry (MS) analysis of nuclear PA levels using nuclear phosphatidylethanolamine (PE) as an internal control, and found that p53 QM expression reduced nuclear PA levels in thymidine-blocked H1299 cells (*i.e.*, reduces the PA/PE ratio) (Fig. 5B). si*CTDNEP1* treatment of these cells largely cancelled the p53-mediated PA reduction (Fig. 5B and Fig. S3A) coupled with a significant increase in the amounts of perinuclear H3K27me3 (Fig. 5, C and D). Thus, collectively, CTDNEP1 appears to function under p53 to reduce nuclear PA levels, and to mitigate the aberrant accumulation of H3K27me3 near the NE. Therefore, it is conceivable to assume that the reduction of nuclear PA levels by the p53-CTDNEP1 axis facilitates the nuclear entry of H3.1 during the G1/S phase. In contrast, if H3.1 molecules trespass into the nucleus in the absence of p53, they may

accumulate near the NE at least transiently, and then be modified to H3K27me3 by EZH2 before forming nucleosomes.

CTDNEP1 increases Lipin in the nucleus

We then found that the nuclear levels of Lipin 1 were increased upon p53 QM expression in thymidine-blocked H1299 cells, and that si*CTDNEP1* canceled this augmentation (Fig. 5E). A biochemical analysis confirmed these results, in which p53 QM increased the amounts of Lipin 1 in the nuclear fraction (Fig. 5F). CTDNEP1 dephosphorylates and hence activates Lipin [21, 22]. The phosphorylation levels of Lipin 1 were unaffected by the presence or absence of p53 QM (Fig. S3B). Therefore, p53 and CTDNEP1 may increase the nuclear levels of Lipin 1. On the other hand, as antibodies against Lipin 2 and Lipin 3 were not available, we were unable to exclude the possible involvement of these isoforms in CTDNEP1 function.

TMEM255A increases CTDNEP1 levels in response to p53

Next, to at least partially understand the mechanism underlying the regulation of the NE by p53, we focused on the association between p53 and CTDNEP1. The *CTDNEP1* promoter does not contain p53-binding sites, and *CTDNEP1* mRNA was not increased by p53 QM in H1299 cells (Fig. S3C). However, si*TP53* reduced CTDNEP1 protein levels in MCF7 cells without reducing its mRNA (Fig. S3, D and E). si*CTDNEP1* also reduced Lipin1 protein levels in H1299 cells (Fig. 6A and Fig. S3A). Therefore, p53 appeared to upregulate CTDNEP1, which may then upregulate Lipin1.

CTDNEP1-regulatory subunit-1 (NEP1R1) increases CTDNEP1 protein levels by binding to CTDNEP1 [21, 22, 24]. However, neither p53 QM nor p53 WT induced *NEP1R1* in H1299 cells (Fig. 6B). We then found that a hitherto poorly characterized gene, namely, *TMEM255A* (also called *FAM70A*), was induced by p53 WT and p53 QM in H1299 cells (Fig. 6C and Table S1). The expression of TMEM255A increased CTDNEP1 levels in reconstitution experiments, in which we used epitope-tagged CTDNEP1 (eCTDNEP1: CTDNEP1-Myc-FLAG or HA-CTDNEP1) and epitope-tagged TMEM255A (eTMEM255A) (Fig. 6D and Fig. S3F). Moreover, eTMEM255A was clearly coprecipitated with eCTDNEP1 (Fig. 6D and Fig. S3F). Furthermore, p53 QM increased eCTDNEP1 levels in H1299 cells, and si*TMEM255A* cancelled this increase (Fig. 6E and Fig. S3G). Therefore, it is likely that p53 induces *TMEM255A*, which then increases CTDNEP1 levels. On the other hand, the degree of the CTDNEP1 increase by the p53-TMEM255A-CTDNEP1 axis appeared to be smaller than what we observed earlier regarding the H3.1 interactome. Thus, mechanisms other than this might also exist by which p53 increases CTDNEP1 in the H3.1 interactome.

Discussion

In this study, we identified nuclear PA as a hitherto unidentified target of p53 function, which is closely associated with the proper nuclear entry and epigenetic modification of H3.1. The main factors responsible for this p53 function appear to be CTDNEP1 and EZH2, in which p53 increases CTDNEP1 and decreases EZH2 in the nuclear H3.1 interactome formed during the G1/S phase (Fig. 6F).

The induction of *TMEM255A* by p53 provided a possible link between p53 and CTDNEP1, and p53 has been previously shown to suppress the *EZH2* gene promoter [25]. Thus, the duality of p53 in transcriptional regulation may underlie the herein identified function of p53. However, many issues remained unidentified, as below. As discussed earlier, the p53-TMEM255A-CTDNEP1 axis may not fully explain the p53-mediated increase in CTDNEP1 level in the H3.1 interactome. Total cellular EZH2 protein levels were not notably changed in H1299 cells by p53 (see Fig. 4A), and hence some unknown mechanism might exist that specifically regulates the amounts of EZH2 in the H3.1 interactome. Whether the *TMEM255A* promoter is a direct target of p53 should also be clarified, as p53 was shown to bind directly to the *TMEM255A* locus in mouse embryonic fibroblasts [26]. Moreover, we showed that H3.1 demonstrates robust affinity to PA. Although mechanisms regulating PA in the nuclear membrane as well as in the nuclear pore complex have been extensively studied [27, 28], the specific mechanisms by which PA constrains H3.1 near the NE awaits to be clarified. Furthermore, the mechanisms as to how EZH2 captures H3.1 molecules in the vicinity

of the NE, and then marks them as repressive before they interact with DNA and form nucleosomes should also be clarified.

Loss of normal p53 in epithelial cells may cause the aberrant deposition of H3K27me3 on epithelial-specific gene loci, such as *CDH1*, and in this process p53 has been shown to employ EZH2 [29, 30]. However, we here found that the aberrant perinuclear accumulation of H3K27me3 also occurs in p53-decient mouse fibroblasts. Thus, the function of p53 to avoid the aberrant H3K27me3 accumulation and to control the H3.1 nuclear entry did not seem to be specific to epithelial cells.

In summary, we clarified that the nucleus tightly controls the entry of H3.1 histones during the G1/S phase, and provided unprecedented perspectives regarding p53, as well as regarding the epigenetic regulation of histones. Our results point out several crucial problems that should be considered in the future, as follows: 1) mechanisms by which EZH2 captures H3.1 molecules that are randomly about to enter the nucleus, before they are utilized to form nucleosomes, 2) whether such aberrantly marked histones will then be discarded from the nucleus, or used somehow in the nucleosomes, 3) whether such a gate-keeping role of the NE is necessary only for G1/S phase-specific H3 histones, and, finally, 4) what is the biological significance of such nuclear control of histone entry.

Materials and methods

Plasmid construction and retroviral gene transduction

A cDNA encoding a p53 protein with quadruple mutations (L22Q/W23S/W53Q/F54S; p53 QM) was generated by PCR-based mutagenesis [31]. The cDNA for p53 WT or p53 QM was cloned together with the DNA sequence for an NH_2-terminal FLAG tag into pRetroX-Tight-Pur (Clontech). Retroviruses with the vesicular stomatitis virus–G (VSV-G) envelope were produced by transfection of GP2-293 cells (Clontech) with the pRetroX construct and pVSV-G (Clontech) using Lipofectamine LTX reagent (Invitrogen), following the manufacturer's instructions. cDNAs encoding CTDNEP1, NEP1R1, and TMEM255A followed by Myc-FLAG tag were purchased from Origene (cat. no. RC203657, RC235833, and RC207956, respectively).

Cell culture

H1299 cells, A549 cells, MCF7 cells, and MB352 cells were obtained from the American Type Culture Collection, and cultured under 5% CO_2 at 37 °C in Dulbecco's modified Eagle's medium supplemented with 10% fetal bovine serum. HMLE cells were cultured in Mammary Epithelial Cell Growth Medium (MEGM) (Lonza). HMLE cells were generated by introducing SV40 large T-antigen and human telomerase reverse transcriptase into a primary culture of normal mammary epithelial cells (Lonza). HMLE cells were cultured in MEGM. No mycoplasma were detected in cultures by 4′,6-diamidino-2-phenylindole or TO-PRO-3 (Thermo Fisher Scientific) staining. Polyclonal cell lines capable of the inducible expression of normal p53 (p53 WT) or a

mutant p53 (p53 QM) were generated by infection of H1299 cells with the corresponding retrovirus and the rtTA retrovirus (Clontech), followed by selection with puromycin (1 μg/mL) and geneticin (G418, 500 μg/mL). The cells were cultured for 48 to 72 h in the presence of doxycycline (0.5 μg/mL) to induce the corresponding genes. Polyclonal cell lines expressing an epitope-tagged CTDNEP1 (MCF7-eCTDNEP1) were generated by the transfection of MCF7 cells with a vector encoding CTDNEP1, followed by selection with geneticin (G418, 250 μg/mL). H1299 and MB352 cells were stably transfected with pPB vectors encoding Fucci probes [32].

Antibodies and reagents

Primary antibodies for immunofluorescence, PLA, and immunoblot analysis were purchased from commercial sources as listed in Table S3. Thymidine (Sigma, #T9250) was used to inhibit S-phase progression. DSP (Dojindo, #D629) was used to crosslink cellular proteins at 1 mM for 30 min at room temperature. Bis(sulfosuccinimidyl)suberate disodium salt (BS3; Dojindo, #B574) was used to crosslink the antibodies to protein G magnetic beads (Cell Signaling Technology). Benzonase (Merck, #70664-3CN) was added to the nuclear extracts at 100 units/mL with 1 mM $MgCl_2$ overnight at 4 °C to digest nucleic acids. Deoxycytidine (Sigma, #D3897) was used to release cells from the thymidine-mediated blockade of cell cycle progression.

Western blotting

Samples were loaded onto e-PAGEL gel (ATTO) or TGX FastCast gel (Bio-Rad), electrophoresed, and then the proteins in the gel were transferred onto Immobilon-FL polyvinylidene difluoride membranes (Millipore). The membranes were blocked with BlockPRO Protein-free Blocking Buffer (Visual Protein) or 1% bovine serum albumin (BSA) and 5% skim milk in phosphate-buffered saline (PBS), and then incubated with primary antibody solution at 4 °C overnight. After washing with PBS containing 0.1% Tween 20 (PBST), the membrane was incubated with IRDye secondary antibodies (LI-COR) or horseradish peroxidase-conjugated secondary antibodies (Jackson ImmunoResearch Laboratories) at room temperature for 1 h. After washing again with PBST, the membrane was scanned with Odyssey Imaging System (LI-COR) or detected with ImageQuant LAS 4000 mini imager (GE Healthcare), followed by reaction with detection reagents (ECL Western Blotting Detection Reagents, GE Healthcare). The primary antibodies and their dilutions are listed in Table S3. All images were processed using Image J and/or Photoshop software.

Cell-cycle analysis

H1299 cells transduced with a vector encoding p53 WT or p53 QM were cultured with or without thymidine for 20 h. Cells were then trypsinized, washed twice in PBS, and fixed with ice-cold 70% ethanol for 2 h. Fixed cells were then washed twice in PBS, incubated with 0.5 mg/mL RNase A (Sigma, #R4642) at 37 °C for 30 min, followed by staining of DNA with 50 μg/mL propidium iodide. Stained cells were subjected to flow cytometric analysis (BD, FACSVerse™).

Immunofluorescence analysis

For immunofluorescence analysis, cells cultured on coverslips were fixed with 4% paraformaldehyde in PBS for 20 min, permeabilized with 0.1% Triton X-100 in PBS for 10 min, and incubated with blocking solution (1% BSA in PBS) for more than 60 min at room temperature. The cells were then incubated with primary antibodies for 60 min at room temperature, then washed with blocking solution and incubated with Alexa Fluor 488-, Alexa Fluor 647-, or Cy3-conjugated secondary antibodies (Molecular Probes) for 30 min. The cells were also stained with TO-PRO-3 dye (Thermo Fisher Scientific) to visualize nuclei. The cells were finally washed with blocking solution, mounted onto glass slides with ProLong Diamond antifade reagent (Thermo Fisher Scientific), and observed using a confocal laser-scanning microscope with an oil-immersion objective (CFI Plan Apo VC 100×/1.4 NA), and analyzed with the attached software (Model A1R with NIS-Elements, Nikon), or with an N-SIM microscope (Nikon) with an oil-immersion objective (100×/1.49 NA), laser illumination, and an electron-multiplying charged-coupled device camera. Image reconstruction was performed using NIS-Elements software (Nikon). All images were processed using Photoshop software.

Proximity ligation assay

To visualize the subcellular localization of the H3K27me3-lamin A/C, H3K27me3-H4, and H3-EZH2 interactions, H1299 cells with or without p53 QM expression were

cultured with thymidine for 20 h to be arrested in the S phase. Cells were then fixed, permeabilized, and incubated with primary antibodies, as described in the immunofluorescence analysis section. PLA reactions were performed using Duolink™ In Situ PLA Probe Anti-Mouse PLUS, Anti-Rabbit MINUS, and Detection Reagents Orange (Sigma), following the manufacturer's instructions. After the ligation and amplification reactions, cells were further incubated with the Alexa Fluor 488-conjugated anti-lamin B1 antibody (Santa Cruz, #sc-365214AF488) and TO-PRO-3 dye to visualize the nuclear lamina (NL) and DNA, respectively. Specificities of the antibodies used for the PLA were confirmed by immunostaining performed at the same concentrations.

Cell cycle synchronization and release

Cells were synchronized at the G1/S border or S phase by a single thymidine block (2 mM thymidine, 18–20 h) and then released by incubation in fresh media containing deoxycytidine (24 μM).

Labeling of newly synthesized DNA

To label and visualize newly replicating DNA, the cells released from the thymidine block by incubation in fresh media containing deoxycytidine (24 μM) for 2 h were quickly rinsed with a hypotonic buffer (10 mM HEPES [pH 7.4] and 50 mM KCl), and incubated in this buffer containing 0.1 mM biotin-dUTP (Roche, #11093070910) for 10 min. Cells were then cultured in fresh culture medium for 20 min before fixation.

Biotin-dUTP incorporated into the DNA replication sites were visualized by Alexa Fluor 488-conjugated streptavidin (Thermo Fisher Scientific, #S32354).

Protein crosslinking and immunoprecipitation

For crosslinking, cells were washed with PBS and incubated with 1 mM DSP in PBS for 30 min at room temperature. Cells were then lysed with cell lysis buffer (10 mM HEPES [pH 7.4], 10 mM KCl, 0.05% NP-40) supplemented with a protease inhibitor cocktail (Merck, #4693116001), and incubated on ice for 20 min. The lysates were then centrifuged at 14,000 rpm for 10 min at 4 °C. The supernatant (cytosolic fraction) was removed and the pellet (nuclei) was resuspended in modified RIPA buffer (50 mM Tris [pH 7.4], 500 mM NaCl, 1 mM EDTA, 1% Triton X-100, 1% SDS, and 1% sodium deoxycholate) supplemented with the protease inhibitor cocktail, bath-sonicated, and incubated on ice for 20 min. The lysates were then centrifuged at 15,000 rpm for 10 min at 4 °C. The supernatant (crosslinked nuclear extracts) was diluted to yield 140 mM NaCl and 0.1% SDS for immunoprecipitation. For immunoprecipitation, normal rabbit IgG or anti-H3 antibodies were crosslinked to protein G magnetic beads by BS3. The crosslinked nuclear extracts were then immunoprecipitated with antibody-conjugated beads overnight at 4 °C. Samples for MS analysis or western blot analysis were prepared by incubating and boiling the beads in SDS sample buffer.

Identification of H3.1-interacting proteins by liquid chromatography-tandem MS (LC-MS/MS)

Samples were reduced with 10 mM TCEP at 100 °C for 10 min, alkylated with 50 mM iodoacetamide at an ambient temperature for 45 min, and then subjected to SDS-PAGE. Electrophoresis was stopped at a migration distance of 2 mm from the top edge of the separation gel. After CBB staining, protein bands were excised, destained, and cut finely prior to in-gel digestion with Trypsin/Lys-C Mix (Promega) at 37 °C for 12 h. The resulting peptides were extracted from gel fragments and analyzed using Orbitrap Fusion Lumos mass spectrometer (Thermo Scientific) combined with UltiMate 3000 RSLC nano-flow HPLC (Thermo Scientific). Peptides were enriched with μ-Precolumn (0.3 mm i.d. × 5 mm, 5 μm, Thermo Scientific) and separated on an AURORA column (0.075 mm i.d. × 250 mm, 1.6 μm, Ion Opticks Pty Ltd.,) using the two-step gradient; 2% to 40% acetonitrile for 110 min, followed by 40% to 95% acetonitrile for 5 min in the presence of 0.1% formic acid. The analytical parameters of Orbitrap Fusion Lumos were set as follows: resolution of full scans = 50,000, scan range (m/z) = 350 to 1,500, maximum injection time of full scans = 50 msec, AGC target of full scans = 4×10^5, dynamic exclusion duration = 30 sec, cycle time of data-dependent MS/MS acquisition = 2 sec, activation type = HCD, detector of MS/MS = ion trap, maximum injection time of MS/MS = 35 msec, AGC target of MS/MS = 1×10^4. The MS/MS spectra were searched against a *Homo sapiens* protein sequence database (20,366 entries) in SwissProt using Proteome Discoverer 2.4 software (Thermo Scientific), in which peptide identification filters were set at a false discovery rate of less than 1%. Label-free relative quantification analysis for proteins was performed with the default parameters of Minora Feature Detector node, Feature Mapper node, and Precursor Ions Quantifier

node in Proteome Discoverer 2.4 software.

Protein lipid overlay assay

Nitrocellulose membranes spotted with serial dilutions of different lipids (Membrane Lipid Arrays, Echelon Biosciences, #P-6003) were used to assess the lipid binding activity of histone H3.1. Membranes were incubated with blocking buffer (3% fatty acid-free BSA [Fujifilm, #017-15141] and 0.1% Tween 20 in PBS) for 1 h at room temperature before being incubated with 1.0 μg/mL of recombinant human histone H3.1 (New England Biolabs, #M2503S) for 1 h at room temperature. The membrane was then washed with 0.1% Tween 20 in PBS, and incubated with an anti-histone H3.1/H3.2 antibody for detection by immunoblotting.

Phosphatase assay

To analyze the phosphorylation status of Lipin 1, cells were lysed with 2× PPase reaction buffer (1× buffer contains 50 mM HEPES [pH 7.5], 100 mM NaCl, 10% glycerol, and 0.5% Triton X-100) supplemented with a protease inhibitor cocktail (Merck, #4693116001). The lysates were then bath-sonicated on ice for 5 min, and centrifuged at 14,000 rpm for 10 min at 4 °C. Total lysates (200 μg each) were incubated with or without 400 U lambda protein phosphatase (New England Biolabs, #P0753S) and 1 mM $MnCl_2$ at 30 °C for 30 min. The reaction was stopped with 5× SDS sample buffer, and boiled for 5 min before western blot analysis.

Quantification of PA in H1299 nuclei by LC-MS/MS

To prepare H1299 cell nuclei, cells were collected and washed with ice-cold PBS on ice. Cells were lysed with a hypotonic buffer (10 mM HEPES [pH 7.4], 1.5 mM $MgCl_2$, and 10 mM KCl) supplemented with 1 mM DTT, a protease inhibitor cocktail (Merck, #4693116001), and a phosphatase inhibitor cocktail (Sigma, #04906837001), and then incubated on ice for 15 min. NP-40 at 0.5% (v/v) was then added to the lysates, briefly vortexed, and centrifuged at 10,000 × g for 40 sec at 4 °C. The supernatant (cytosolic fraction) was removed and the pellet (nuclei) was resuspended in the hypotonic buffer (10 mM HEPES [pH 7.4], 1.5 mM $MgCl_2$, and 10 mM KCl) supplemented with 1 mM DTT, the protease inhibitor cocktail, and the phosphatase inhibitor cocktail. The nuclei were then centrifuged at 10,000 × g for 40 sec at 4 °C, washed twice with ice-cold PBS, and then subjected to lipid extraction.

A 50 μL methanol solution containing 20 pmol each of C15:0/18:1 PA (Avanti polar lipids, #330721) and C12:0/13:0 PE (Avanti polar lipids, #LM1100) were added to each nuclear sample in 1.2 mL methanol in a glass tube, followed by the addition of ultrapure water (400 μL), 2 M HCl (400 μL), and 1 M NaCl (200 μL). After vigorous vortex-mixing, 2 mL $CHCl_3$ was added followed by further vortexing for 1 min. After centrifugation (1,200 × *g* for 3 min at room temperature), the lower organic phase (crude lipid extract) was collected and transferred to a new glass tube. Purified phospholipids were derivatized by methylation using a method described previously [33]. Briefly, 150 μL of 0.6 M (trimethylsilyl)diazomethane (Tokyo Chemical Industry, #T1146) was added to the purified phospholipid fraction prepared as above at room

temperature. After 10 min, the reaction was quenched with 10 μL glacial acetic acid. The samples were mixed with 400 μL $CHCl_3$ and 400 μL ultrapure water followed by vortexing for 1 min. After centrifugation at 1,200 × g for 3 min, the lower phase was dried under a stream of nitrogen, and redissolved in 100 μL acetonitrile.

LC-MS/MS was performed using a triple quadruple mass spectrometer QTRAP6500 (ABSciex) and a Nexera X2 HPLC system (Shimadzu) combined with a PAL HTC-xt (CTC Analytics) autosampler. The mass range of the instrument was set at 5 to 2,000 *m/z*. Spectra were recorded in the positive ion mode as $[M+H]^+$ ions for the detection of PAs and PEs. The ion spray voltage was set at 5.5 kV, cone voltage at 30 V, and source block temperature at 100 °C. Curtain gas was set at 20 psi, collision gas at 9 psi, ion source gas pressures 1/2 at 50 psi, declustering potential at 100 V, entrance potential at 10 V, collision cell exit potential at 12 V, and collision energy values at 35 eV. Lipid samples (10 μL each) dissolved in acetonitrile were injected using the autosampler, and molecules were separated using a Bio C18 column (1.9 μm, 2.1 × 150 mm) at 60 °C. LC was operated at a flow rate of 100 μL/min with a gradient as follows: 90% mobile phase A (methanol/acetonitrile/deionized water = 18/18/4 containing 5 mM ammonium acetate) and 10% mobile phase B (2-propanol containing 5 mM ammonium acetate) were held for 2 min, linearly increased to 82% mobile phase B over 17 min, and held at 85% mobile phase B for 4 min. The column was re-equilibrated to 10% mobile phase B for 10 min before the next injection. Data were analyzed by MultiQuant 3.0.2 software (ABSciex). Concentrations of each molecular species were calculated by dividing the peak area of each species with the peak area of the corresponding internal surrogate

standard. The sum of each phospholipid molecular species was calculated, and the ratio (PA/PE) was presented in the figure.

RNA interference (RNAi) experiments

Silencer Select or Silencer Pre-designed siRNAs targeting coding sequences of human *TP53* mRNA (5′-GUAAUCUACUGGGACGGAATT-3′: p53 #1, and 5′-GGUGAACCUUAGUACCUAATT-3′: p53 #2), human *CTDNEP1* mRNA (5′-GUACCAAACUGUUCGAUAUTT-3′: CTDNEP1 #1, and 5′-GGAUCUGGAUGAGACACUUTT-3′: CTDNEP1 #2), human *LPIN1* mRNA (5′-GACUUUCCCUGUUCGGAUATT-3′: LPIN1 #1, and 5′-GGAGUGUCUUUGAAUAGAATT-3′: LPIN1 #2), human *TMEM255A* mRNA (5′-AAACCUUAUUGAGAACAAATT-3′: TMEM255A #1, and 5′-GGCUUUAAGGACAUGAACCTT-3′: TMEM255A #2), or Stealth siRNAs targeting coding sequences of human *EZH2* mRNA (5′-GACCACAGUGUUACCAGCAUUUGGA-3′: EZH2 #1, and 5′-GAGCAAAGCUUACACUCCUUUCAUA-3′: EZH2 #2) were obtained from Thermo Fisher Scientific. Silencer Select negative control siRNA and Stealth negative control siRNA were purchased from Thermo Fisher Scientific. For the transfection of siRNA, cells were plated at 15% to 20% confluence in 6-well plates together with 15 nM Silencer Select or Silencer Pre-designed siRNA and 3.5 μL of RNAi MAX (Thermo Fisher Scientific), or with 150 pmol of Stealth siRNA and 3.5 μL of RNAi MAX. They were then cultured in complete medium for 24 h before a second round of siRNA

transfection.

Quantitative reverse transcription (RT)-PCR analysis

Total RNA was extracted from cells using Trizol reagent (Thermo Fisher Scientific), purified with Direct-zol RNA Miniprep kit (Zymo Research), and aliquots (1 μg) of the RNA were subjected to RT with SuperScript IV polymerase (Thermo Fisher Scientific). TaqMan RT-PCR primers for *NEP1R1*, *TMEM255A*, *CTDNEP1*, and *ACTB* were obtained from Applied Biosystems for quantitative PCR analysis. Quantitative PCR analysis was performed using the 7300 Fast Real-Time PCR System (Applied Biosystems). For quantification of *NEP1R1*, *TMEM255A*, *CTDNEP1*, or *ACTB*, absolute quantification was performed using plasmids encoding human *NEP1R1*, *TMEM255A*, *CTDNEP1*, or *ACTB* as a standard.

RNA-Seq for H1299 cells

Total RNA was isolated from each sample using Direct-zol RNA MiniPrep Kit (Zymo Research) together with DNase I treatment. The integrity and quantity of the total RNA was measured using an Agilent 2100 Bioanalyzer RNA 6000 Nano Kit (Agilent Technologies). Total RNA obtained from each sample was subjected to sequencing library construction using NEBNext Ultra Directional RNA Library Prep Kit for Illumina (New England Biolabs) with NEBNext Poly(A) mRNA Magnetic Isolation Module according to the manufacturer's protocol. The quality of the libraries was assessed using an Agilent 2100 Bioanalyzer High Sensitivity DNA Kit (Agilent

Technologies). The pooled libraries of the samples were sequenced using NextSeq 500 (Illumina, Inc.) in 76-base-pair single-end reads. Sequencing adaptors, low-quality reads, and bases were trimmed with Trimmomatic-0.32 tool [34]. The sequence reads were aligned to the human reference genome (hg19) using Tophat 2.1.1 (bowtie2-3.2.0) [35], which can adequately align reads onto the location including splice sites in the genome sequence. Files of the gene model annotations and known transcripts, which are necessary for whole transcriptome alignment with Tophat, were downloaded from Illumina's iGenomes website (http://support.illumina.com/sequencing/sequencing_software/igenome.html). The aligned reads were subjected to downstream analyses using StrandNGS 3.2 software (Agilent Technologies). The read counts allocated for each gene and transcript (RefSeq Genes 2015.10.05) were quantified using the Trimmed Mean of M-value (TMM) method [36].

Statistical analysis

Statistical analysis was performed using GraphPad Prism 6 software (GraphPad Software, Inc.). Quantitative data are presented as the mean ± standard error of the mean. The sample size for each experiment and the replicate number of experiments are indicated in the figure or figure legends. Comparisons between two groups or more than two groups were performed using the Student *t*-test or one-way ANOVA followed by Dunnett's multiple comparisons test, respectively. Statistical significance was indicated in the figure or figure legends. A *P*-value of less than 0.05 was considered to indicate a

statistically significant difference between groups.

Acknowledgments

We thank H.A. Popiel for her critical reading of the manuscript.

This work was supported by JSPS KAKENHI grant numbers JP20K07305, JP20H05523, and JP16H06280 (to T.O.); JP18H02608 and JP21H02675 (to H.S.); JP20H03206 (to J.H.); JP20H04920 (to J.S.); JP20H03433 (to T.S.); and by AMED grant 18gm0710002h0006 (to T.S.).

Author contributions

T.O. conceived the project and performed the imaging and biochemical experiments. A.H. performed the flow cytometric analysis. Y.O. generated the Fucci constructs and provided instruction on the PLA experiments. N.O. and K.U. performed the MS of the binding proteins of H3.1 and analyzed the data. J.H., J.S., and T.S. performed the MS of the nuclear lipids and analyzed the data. T.O. wrote the manuscript. H.S. supervised the project and modified the manuscript.

Declaration of interests

The authors declare no competing interests in association with this study.

References

1. Alvarez, F. *et al*. Sequential establishment of marks on soluble histones H3 and H4. *J. Biol. Chem.* **286**, 17714-17721 (2011).
2. Apta-Smith, M.J., Hernandez-Fernaud, J.R. & Bowman, A.J. Evidence for the nuclear import of histones H3.1 and H4 as monomers. *EMBO J.* **37** (2018).
3. Pardal, A.J. & Bowman, A.J. A specific role for importin-5 and NASP in the import and nuclear hand-off of monomeric H3. *eLife* **11**, e81755 (2022).
4. Campos, E.I. *et al*. The program for processing newly synthesized histones H3.1 and H4. *Nat. Struct. Mol. Biol.* **17**, 1343-1351 (2010).
5. Campos, E.I. *et al*. Analysis of the histone H3.1 interactome: A suitable chaperone for the right event. *Mol. Cell* **60**, 697-709 (2015).
6. Tyler, J.K. *et al*. The RCAF complex mediates chromatin assembly during DNA replication and repair. *Nature* **402**, 555-560 (1999).
7. Groth, A. *et al*. Human Asf1 regulates the flow of S phase histones during replicational stress. *Mol. Cell* **17**, 301-311 (2005).
8. Mühlhäusser, P., Müller, E.-C., Otto, A. & Kutay, U. Multiple pathways contribute to nuclear import of core histones. *EMBO Rep.* **2**, 690-696 (2001).
9. Soniat, M., Cağatay, T. & Chook, Y.M. Recognition elements in the histone H3 and H4 tails for seven different importins. *J. Biol. Chem.* **291**, 21171-21183 (2016).
10. Mendiratta, S., Gatto, A. & Almouzni, G. Histone supply: Multitiered regulation ensures chromatin dynamics throughout the cell cycle. *J. Cell Biol.* **218**, 39-54 (2019).
11. Tagami, H., Ray-Gallet, D., Almouzni, G. & Nakatani, Y. Histone H3.1 and H3.3 complexes mediate nucleosome assembly pathways dependent or independent of DNA synthesis. *Cell* **116**, 51-61 (2004).
12. Liu, W.H., Roemer, S.C., Port, A.M. & Churchill, M.E. CAF-1-induced oligomerization of histones H3/H4 and mutually exclusive interactions with Asf1 guide H3/H4 transitions among histone chaperones and DNA. *Nucleic Acids Res.* **40**, 11229-11239 (2012).
13. Ungricht, R. & Kutay, U. Mechanisms and functions of nuclear envelope

remodelling. *Nat. Rev. Mol. Cell Biol.* **18**, 229-245 (2017).

14. Barger, S.R., Penfield, L. & Bahmanyar, S. Coupling lipid synthesis with nuclear envelope remodeling. *Trends Biochem. Sci.* **47**, 52-65 (2021).
15. Sakaue-Sawano, A. *et al.* Visualizing spatiotemporal dynamics of multicellular cell-cycle progression. *Cell* **132**, 487-498 (2008).
16. el-Deiry, W.S. *et al.* WAF1, a potential mediator of p53 tumor suppression. *Cell* **75**, 817-825 (1993).
17. Venot, C., Maratrat, M., Sierra, V., Conseiller, E. & Debussche, L. Definition of a p53 transactivation function-deficient mutant and characterization of two independent p53 transactivation subdomains. *Oncogene* **18**, 2405-2410 (1999).
18. Maya-Mendoza, A., Olivares-Chauvet, P., Kohlmeier, F. & Jackson, D.A. Visualising chromosomal replication sites and replicons in mammalian cells. *Methods* **57**, 140-148 (2012).
19. Alabert, C. *et al.* Nascent chromatin capture proteomics determines chromatin dynamics during DNA replication and identifies unknown fork components. *Nat. Cell Biol.* **16**, 281-293 (2014).
20. Cao, R. *et al.* Role of histone H3 lysine 27 methylation in Polycomb-group silencing. *Science* **298**, 1039-1043 (2002).
21. Han, S. *et al.* Nuclear envelope phosphatase 1-regulatory subunit 1 (formerly TMEM188) is the metazoan Spo7p ortholog and functions in the lipin activation pathway. *J. Biol. Chem.* **287**, 3123-3137 (2012).
22. Su, W.-M., Han, G.-S. & Carman, G.M. Yeast Nem1-Spo7 protein phosphatase activity on Pah1 phosphatidate phosphatase is specific for the Pho85-Pho80 protein kinase phosphorylation sites. *J. Biol. Chem.* **289**, 34699-34708 (2014).
23. Bahmanyar, S. & Schlieker, C. Lipid and protein dynamics that shape nuclear envelope identity. *Mol. Biol. Cell* **31**, 1315-1323 (2020).
24. Jacquemyn, J. *et al.* Torsin and NEP1R1-CTDNEP1 phosphatase affect interphase nuclear pore complex insertion by lipid-dependent and lipid-independent mechanisms. *EMBO J.* **40**, e106914 (2021).
25. Tang, X. *et al.* Activated p53 suppresses the histone methyltransferase EZH2 gene. *Oncogene* **23**, 5759-5769 (2004).
26. Kenzelmann Broz, D. *et al.* Global genomic profiling reveals an extensive p53-regulated autophagy program contributing to key p53 responses. *Genes Dev.*

27, 1016-1031 (2013).

27. Romanauska, A. & Köhler, A. The inner nuclear membrane is a metabolically active territory that generates nuclear lipid droplets. *Cell* **174**, 700-715.e718 (2018).
28. Thaller, D.J. *et al.* Direct binding of ESCRT protein Chm7 to phosphatidic acid–rich membranes at nuclear envelope herniations. *J. Cell Biol.* **220**, e202004222 (2021).
29. Oikawa, T. *et al.* Necessity of p53-binding to the CDH1 locus for its expression defines two epithelial cell types differing in their integrity. *Sci. Rep.* **8**, 1595 (2018).
30. Oikawa, T., Otsuka, Y. & Sabe, H. p53-Dependent and -Independent Epithelial Integrity: Beyond miRNAs and Metabolic Fluctuations. *Cancers (Basel)* **10** (2018).
31. Hashimoto, A. *et al.* P53- and mevalonate pathway-driven malignancies require Arf6 for metastasis and drug resistance. *J. Cell Biol.* **213**, 81-95 (2016).
32. Onodera, Y., Nam, J.-M., Horikawa, M., Shirato, H. & Sabe, H. Arf6-driven cell invasion is intrinsically linked to TRAK1-mediated mitochondrial anterograde trafficking to avoid oxidative catastrophe. *Nat. Commun.* **9**, 2682 (2018).
33. Morioka, S. *et al.* A mass spectrometric method for in-depth profiling of phosphoinositide regioisomers and their disease-associated regulation. *Nat. Commun.* **13**, 83 (2022).
34. Bolger, A.M., Lohse, M. & Usadel, B. Trimmomatic: a flexible trimmer for Illumina sequence data. *Bioinformatics* **30**, 2114-2120 (2014).
35. Langmead, B. & Salzberg, S.L. Fast gapped-read alignment with Bowtie 2. *Nat. Methods* **9**, 357-359 (2012).
36. Robinson, M.D. & Oshlack, A. A scaling normalization method for differential expression analysis of RNA-seq data. *Genome Biol.* **11**, R25 (2010).
37. Fischer, M. Census and evaluation of p53 target genes. *Oncogene* **36**, 3943-3956 (2017).
38. Hermeking, H. *et al.* 14-3-3 σ is a p53-regulated inhibitor of G2/M progression. *Mol. Cell* **1**, 3-11 (1997).
39. Kastan, M.B. *et al.* A mammalian cell cycle checkpoint pathway utilizing p53 and GADD45 is defective in ataxia-telangiectasia. *Cell* **71**, 587-597 (1992).

40. Jackson, R.S., 2nd, Cho, Y.J., Stein, S. & Liang, P. CYFIP2, a direct p53 target, is leptomycin-B sensitive. *Cell Cycle* **6**, 95-103 (2007).
41. Muller, M. *et al.* p53 activates the CD95 (APO-1/Fas) gene in response to DNA damage by anticancer drugs. *J. Exp. Med.* **188**, 2033-2045 (1998).
42. Wu, G.S. *et al.* KILLER/DR5 is a DNA damage-inducible p53-regulated death receptor gene. *Nat. Genet.* **17**, 141-143 (1997).
43. Suzuki, S. *et al.* Phosphate-activated glutaminase (GLS2), a p53-inducible regulator of glutamine metabolism and reactive oxygen species. *Proc. Natl. Acad. Sci. U. S. A.* **107**, 7461-7466 (2010).
44. Hu, W. *et al.* Glutaminase 2, a novel p53 target gene regulating energy metabolism and antioxidant function. *Proc. Natl. Acad. Sci. U. S. A.* **107**, 7455-7460 (2010).
45. Liu, G. & Chen, X. The ferredoxin reductase gene is regulated by the p53 family and sensitizes cells to oxidative stress-induced apoptosis. *Oncogene* **21**, 7195-7204 (2002).
46. Bensaad, K. *et al.* TIGAR, a p53-inducible regulator of glycolysis and apoptosis. *Cell* **126**, 107-120 (2006).

Figure legends

Figure 1. p53 suppresses perinuclear H3K27me3 during the G1/S phase. A, Representative SIM images showing the localization of H3K4me3, H3K27ac, or H3K27me3 (red), p53 (green), and DNA (blue). Bars, 10 µm. **B**, Depth-coded alpha-blending views of H3K27me3 from the 3D-SIM images are shown. Bar, 10 µm. **C**, Quantification of cells with perinuclear H3K27me3 accumulation. n = 3 biological replicates, ≥ 100 cells per replicate; ***P = 0.0006, *P < 0.03. **D**, Representative immunoblots of the indicated antibodies. **E**, Representative SIM images show the localization of H3K4me3, H3K27ac, or H3K27me3 (magenta) and DNA (green). Bars, 10 µm. **F**, Representative SIM images show the localization of H3K27me3 (blue). Bars, 10 µm. **G**, Quantification of the cells with perinuclear H3K27me3 accumulation. AS, asynchronous. n = 3 biological replicates, ≥ 50 cells per replicate; ****P < 0.0001, ***P < 0.001, and **P < 0.01. **H**, Representative immunoblots of the indicated antibodies. **I**, Representative confocal images show the localization of H3K27me3 (red), FLAG (green), and DNA (blue). Bars, 10 µm. **J**, Representative SIM images showing the localization of the PLA signals between H3K27me3 and lamin A/C (red), lamin B1 (green), and DNA (blue). Bars, 10 µm. **K**, Quantification of the PLA spots that overlap with perinuclear lamin B1 in each nucleus. n = 3 biological replicates, ≥ 60 nuclei; ****P < 0.0001.

Figure 2. Perinuclear H3K27me3 does not form nucleosomes. A, **B**, Representative SIM images show the localization of H3K27me3 (magenta) and lamin A/C (green) (**A**),

or H3K27me3 (magenta) and DNA (green) (**B**). Enlarged images of the white boxed areas are shown on the right. Pixel intensities on the traversing white lines (1 and 2) are shown at the bottom. Bars, 10 µm. **C**, Representative SIM images show the localization of H3K27me3 (red), biotin-dUTP (green), and DNA (blue). The white boxed area is enlarged on the right. Bars, 10 µm. **D**, Quantification of the colocalization of H3K27me3 and dUTP. n = 2 biological replicates; ****$P < 0.0001$. **E**, Representative SIM images show the localization of the PLA signals between H3K27me3 and H4 (red), lamin B1 (green), and DNA (blue). Bars, 10 µm. **F**, Quantification of the PLA spots that overlap with perinuclear lamin B1 in each nucleus. n = 3 biological replicates; ≥ 60 nuclei; NS, not significant.

Figure 3. H3.1/H3.2 accumulates in the NL during the G1/S phase in the absence of p53. A, Representative immunoblots of the indicated antibodies. AS, asynchronous. **B**, **C**, Representative SIM images show the localization of H3.1/H3.2 (red), lamin B1 (green), and H3.3 (blue) in the absence (**B**) or presence (**C**) of p53 QM. Pixel intensities on the traversing white lines (1, 2, and 3) are shown at the bottom. Bars, 10 µm. **D**, Schematic representation of H3 immunoprecipitation followed by quantitative MS analysis. **E**, Representative proteins identified from the MS analysis. The relative abundance of these proteins is presented as a ratio (Log_2) in the presence/absence of p53 QM.

Figure 4. p53 reduces the proximity between EZH2 and H3 on the NL. A,

Representative immunoblots of the indicated antibodies. IP, immunoprecipitation. **B**, Representative confocal images show the localization of H3K27me3 (red), EZH2 (green), and DNA (blue). Bars, 10 µm. **C**, Representative immunoblots of the indicated antibodies. **D**, Representative SIM images show the localization of PLA signals between H3 and EZH2 (red), lamin B1 (green), and DNA (blue). Bars, 10 µm. **E**, Quantification of the PLA spots that overlap with perinuclear lamin B1 in each nucleus. n = 3 biological replicates, ≥ 60 nuclei; ****$P < 0.0001$.

Figure 5. p53 and CTDNEP1 reduce nuclear PA levels by increasing Lipin 1 in the nucleus. A, H3.1-lipid interactions clarified by membrane lipid arrays. The membrane was spotted with the indicated amount of the following lipids: diacylglycerol (DAG); phosphatidic acid (PA); phosphatidylserine (PS); phosphatidylinositol (PI); phosphatidylethanolamine (PE); phosphatidylcholine (PC); phosphatidylglycerol (PG); and sphingomyelin (SM). **B**, Absolute quantification of PA and PE in the nuclei. PA/PE ratios are indicated. n = 3 or 4 biological replicates; *$P < 0.05$; NS, not significant. **C**, Representative SIM images showing the localization of H3K27me3 (red), lamin B1 (green), and DNA (blue). Bars, 10 µm. **D**, Quantification of the cells with perinuclear H3K27me3 accumulation. n = 4 biological replicates, ≥ 100 cells per replicate; ****$P < 0.0001$, *$P < 0.05$. **E**, Representative confocal images showing the localization of Lipin 1 (green) and DNA (blue). Bars, 10 µm. **F**, Representative immunoblots of the indicated antibodies. Normalized Lipin 1/lamin B1 ratios are shown. n = 3 biological replicates; **$P < 0.01$.

Figure 6. TMEM255A increases CTDNEP1 downstream of p53. A, Representative immunoblots using the indicated antibodies. Normalized Lipin 1/β-tubulin ratios are shown. n = 3 biological replicates; $^{**}P < 0.01$, $^{*}P < 0.05$; NS, not significant. **B**, **C**, Quantification of *NEP1R1* (**B**) or *TMEM255A* (**C**) mRNA (normalized by *ACTB* mRNA). n ≥ 3 biological replicates; $^{**}P < 0.01$, $^{*}P < 0.03$; NS, not significant. **D**, Representative immunoblots using the indicated antibodies. IP, immunoprecipitation. **E**, Representative immunoblots using the indicated antibodies. V, vehicle. Normalized eCTDNEP1/β-tubulin ratios are shown. n = 3 biological replicates; $^{**}P < 0.01$. **F**, Model for the nuclear entry of H3.1 regulated by p53.

Supplemental information

Supplementary figure legends

Figure S1. Loss of p53 induces H3K27me3 accumulation in the perinuclear region, and p53 QM does not delay cell cycle progression in H1299 and MB352 cells. A, Representative SIM images show the localization of H3K4me3, H3K27ac, or H3K27me3 (red), p53 (green), and DNA (blue). Bars, 10 µm. **B**, Domain structure of p53. The human p53 QM mutant used in this study harbors the L22Q/W23S/W53Q/F54S mutations (indicated as *) in the transactivation domain. **C**, Representative flow cytometry histograms are shown. Cells in the G1/S phase are defined as those under the black horizontal bar, and their proportions are indicated.

Figure S2. Changes in the expression levels of p53-target genes upon p53 WT or p53 QM expression in H1299 cells. Genes identified by RNA-Seq analysis were listed according to the Gene Ontology term that includes "p53". Some other genes were also listed according to the literature [37]. The fold changes (Log_2) to the control are indicated. The expression of p53 WT but not p53 QM induces a wide range of known p53-target genes, such as those implicated in cell cycle arrest (e.g., *CDKN1A* encoding p21/Cip1 [16], *SFN* encoding 14-3-3 sigma [38], and *GADD45A* [39]), apoptosis (e.g., *CYFIP2* [40], *FAS* [41], and *TNFRSF10B* encoding DR5 [42]), and metabolism (e.g., *GLS2* [43, 44], *FDXR* [45], and *TIGAR* [46]).

Figure S3. p53 increases CTDNEP1 via upregulating *TMEM255A*. A, Quantification

of *CTDNEP1* mRNA (normalized by *ACTB* mRNA). n = 3 biological replicates; $^{**}P < 0.01$. **B**, Representative immunoblots using the indicated antibodies. λPP, lambda protein phosphatase. **C**, Quantification of *CTDNEP1* mRNA (normalized by *ACTB* mRNA). n = 3 biological replicates; NS, not significant. **D**, Representative immunoblots for the indicated antibodies. Normalized eCTDNEP1/β-tubulin or eCTDNEP1/GAPDH ratios are shown. n = 3 biological replicates; $^{****}P < 0.0001$. **E**, Quantification of *CTDNEP1* mRNA (normalized by *ACTB* mRNA). n = 3 biological replicates; NS, not significant. **F**, Representative immunoblots using the indicated antibodies. IP, immunoprecipitation. **G**, Quantification of *TMEM255A* mRNA (normalized by *ACTB* mRNA). n = 3 biological replicates; $^{*}P < 0.05$.

Supplementary table legends

Table S1. List of genes upregulated or downregulated upon the expression of p53 WT or p53 QM in H1299 cells

Table S2. H3.1 interacting proteins identified by mass spectrometry analysis

Table S3. List of antibodies used in this study

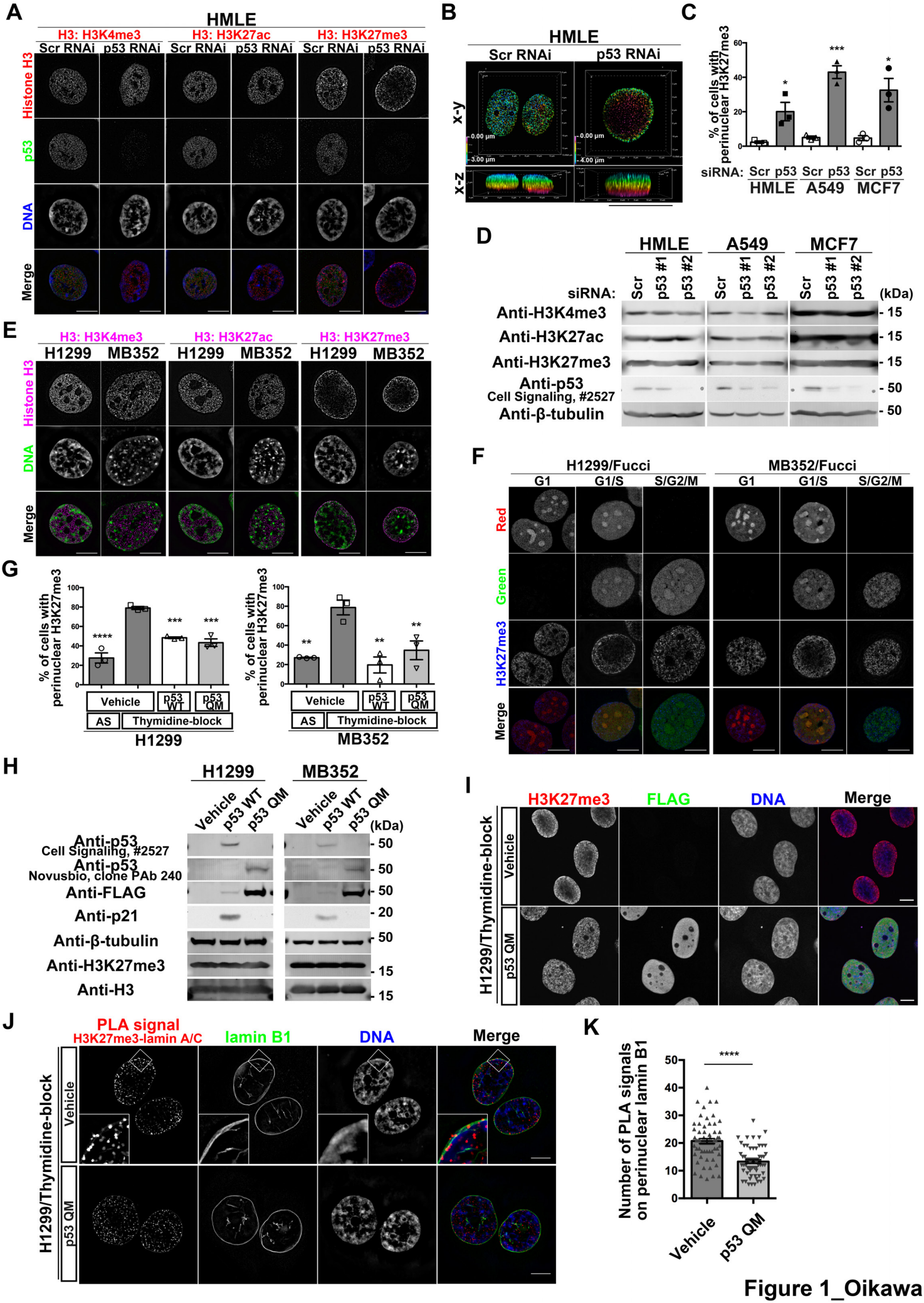

Figure 1_Oikawa

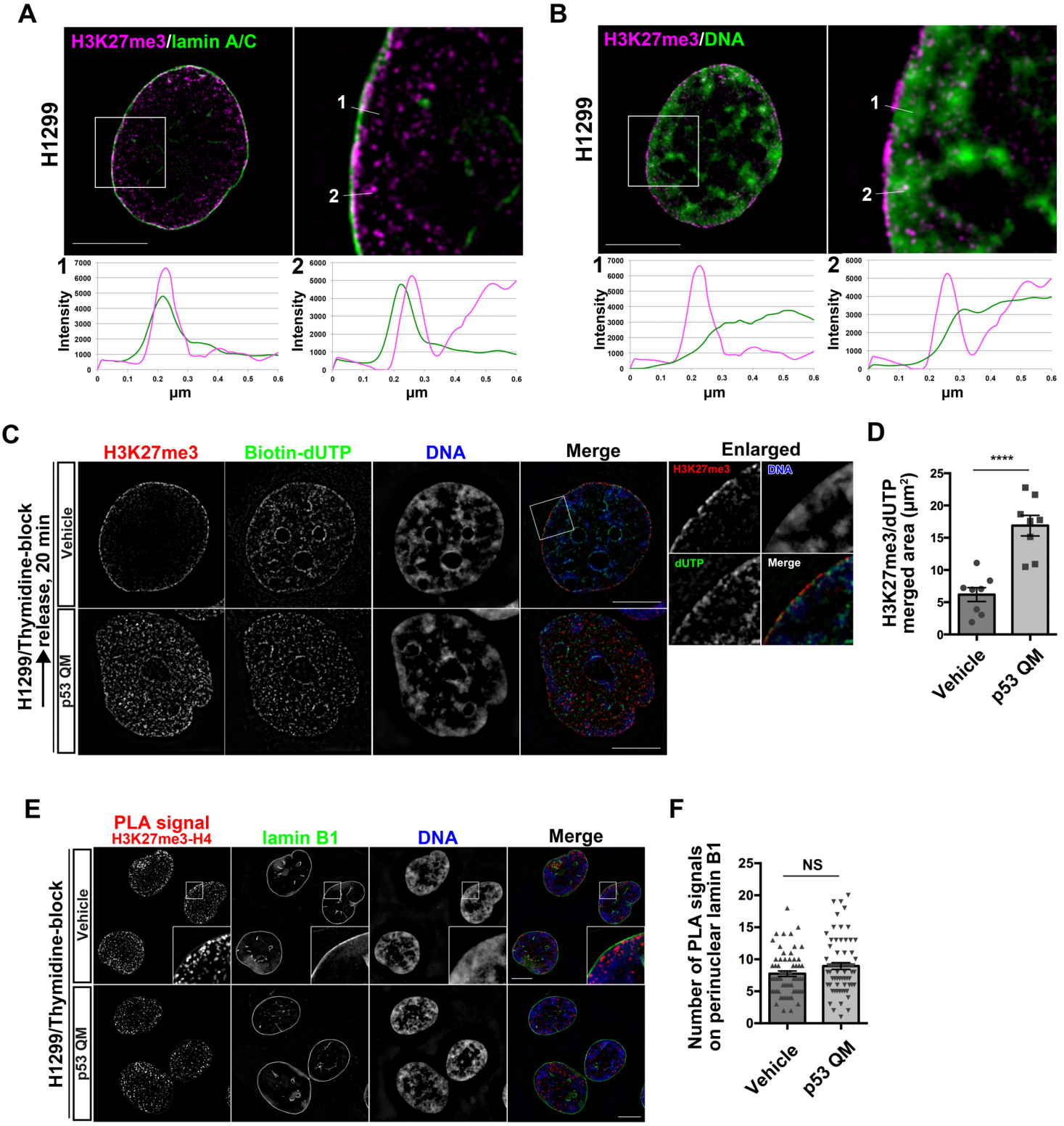

Figure 2_Oikawa

Figure 3_Oikawa

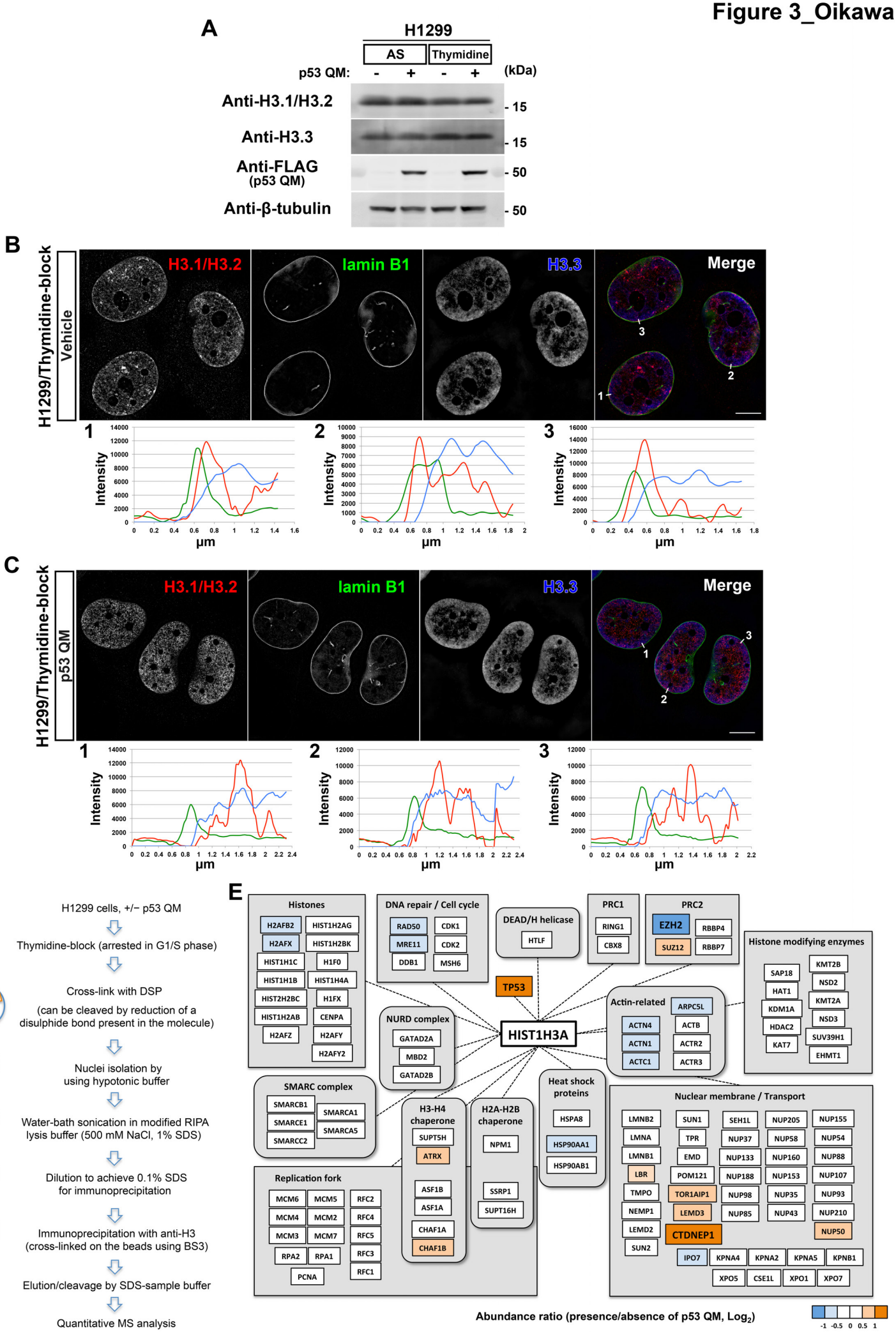

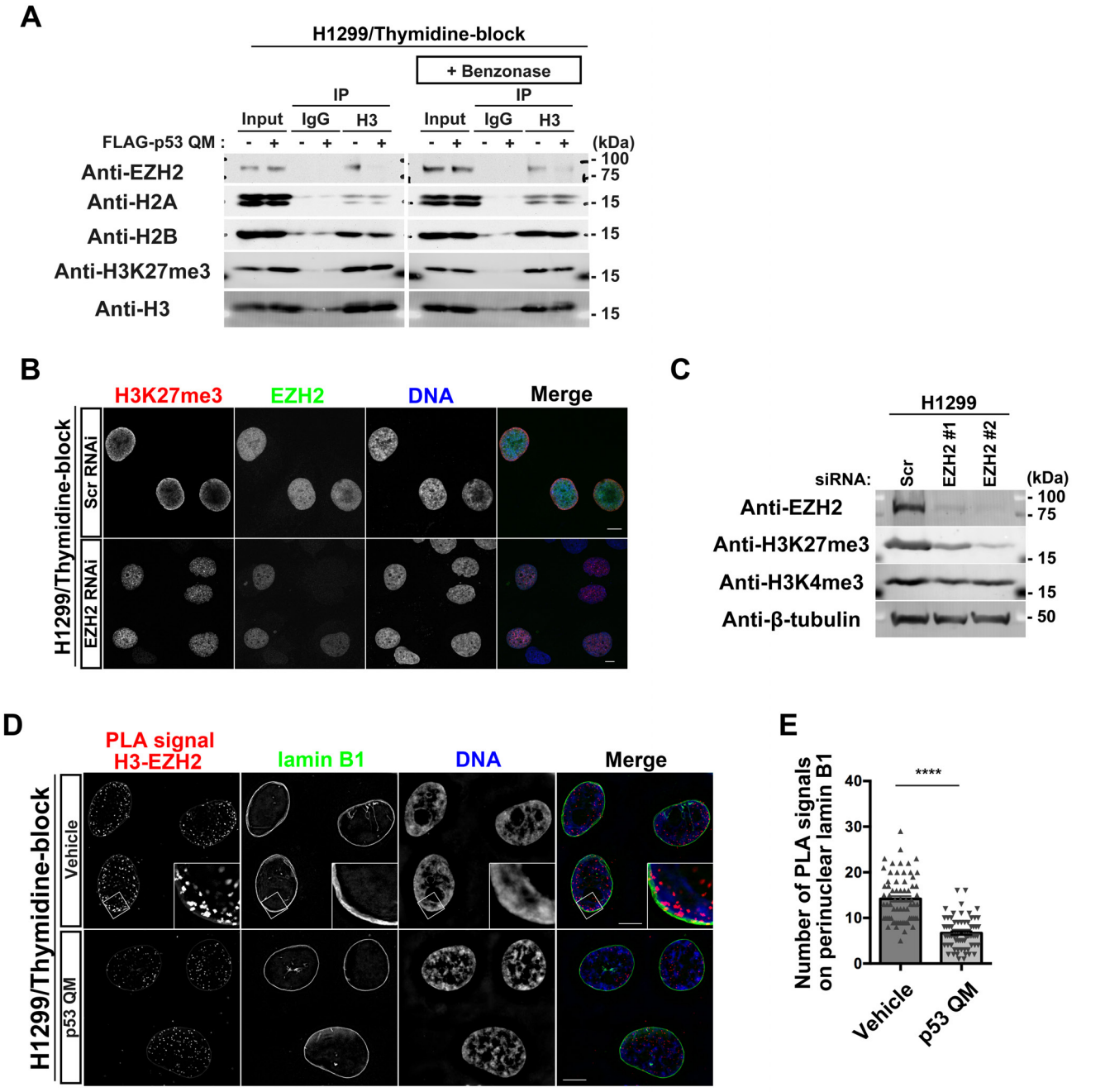

Figure 4_Oikawa

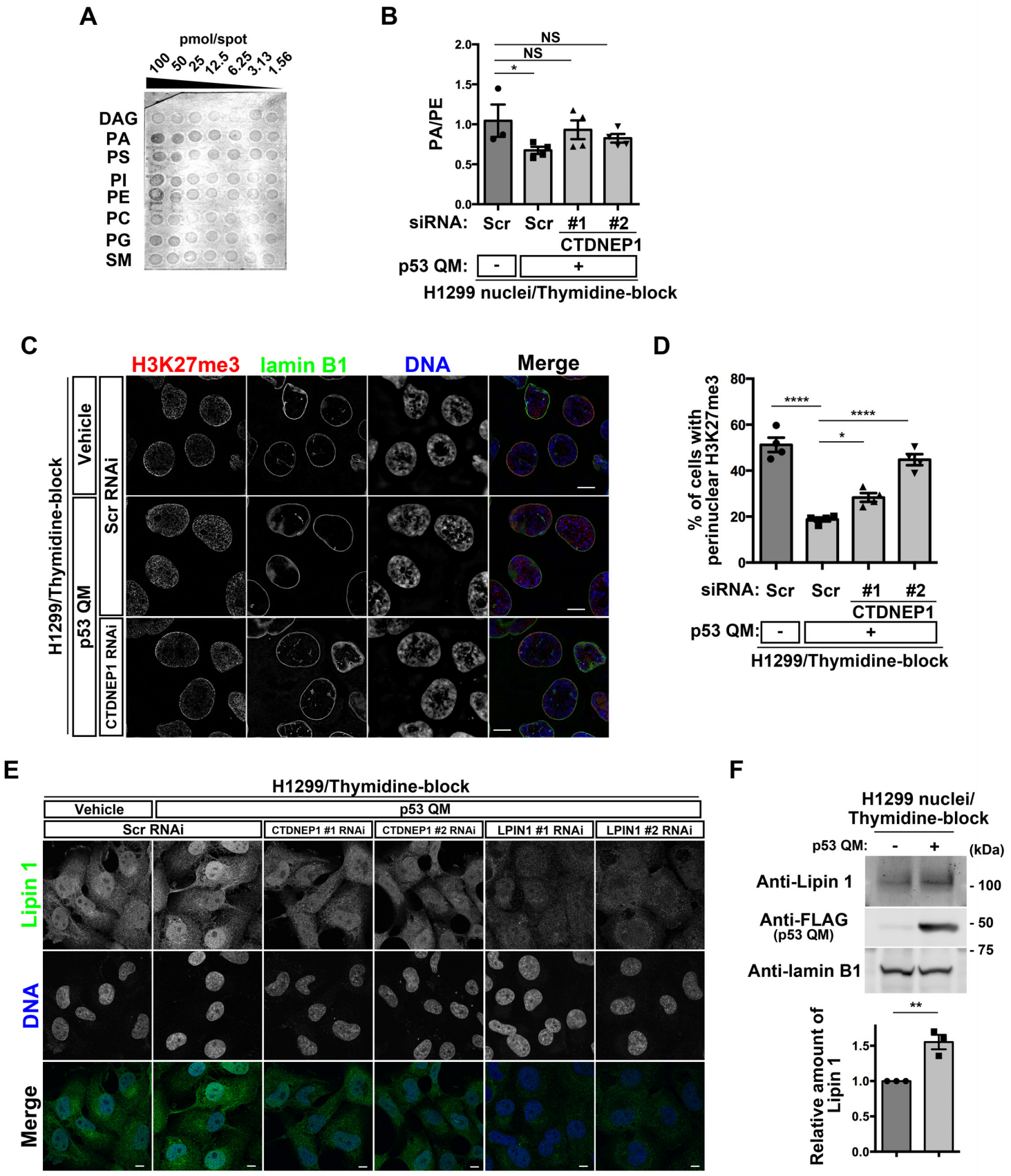

Figure 5_Oikawa

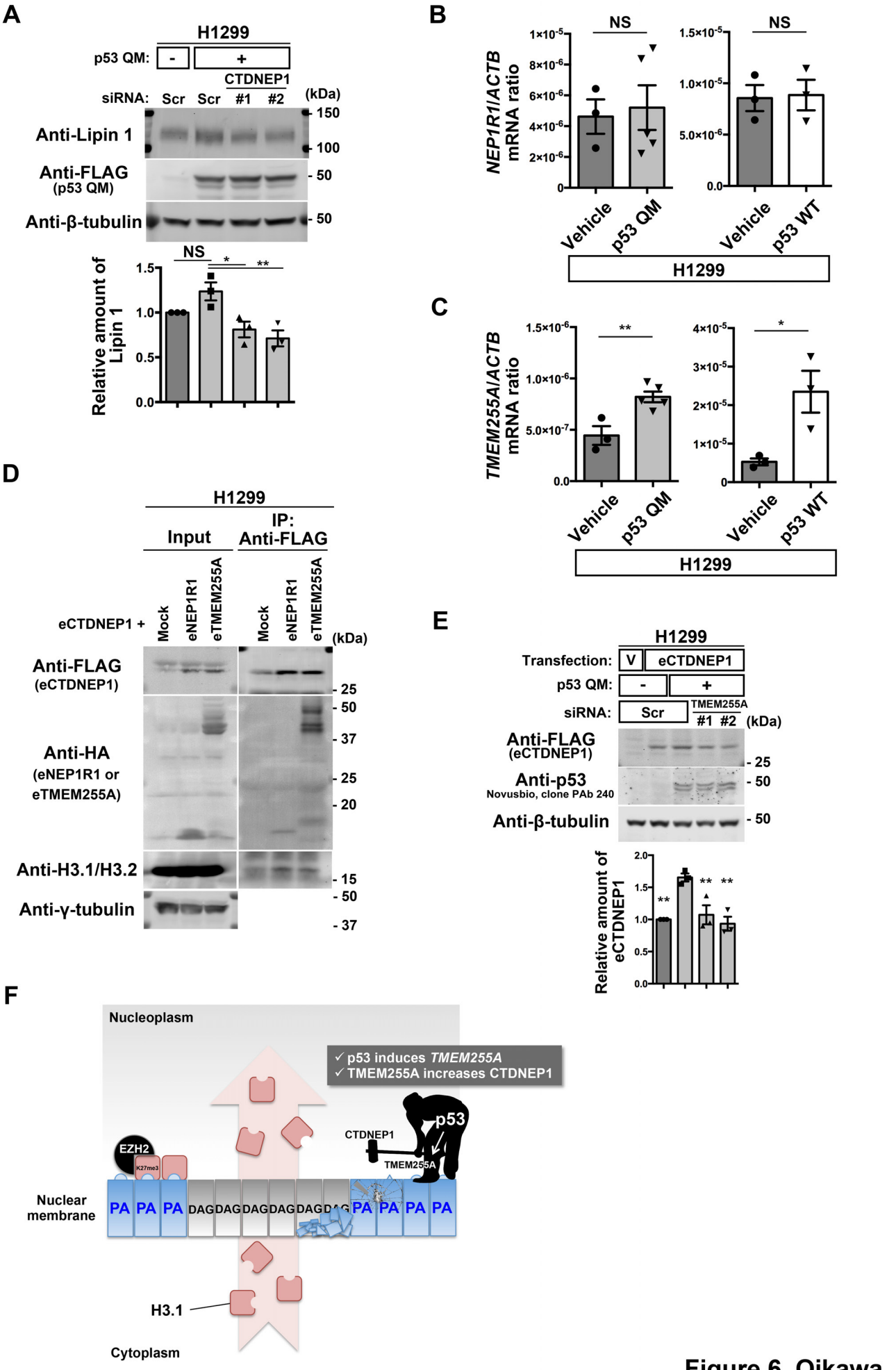

Figure 6_Oikawa

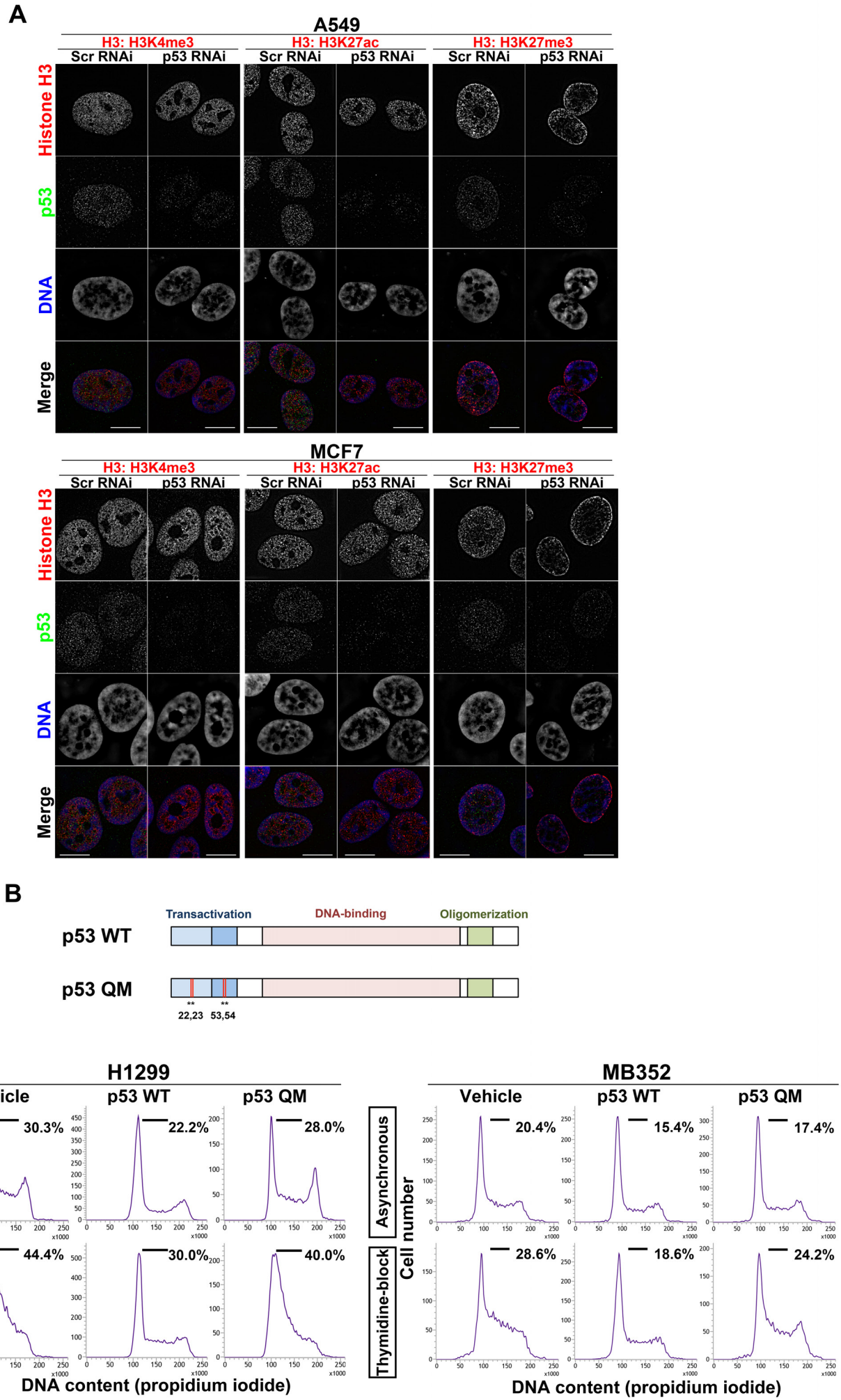

Figure S1_Oikawa

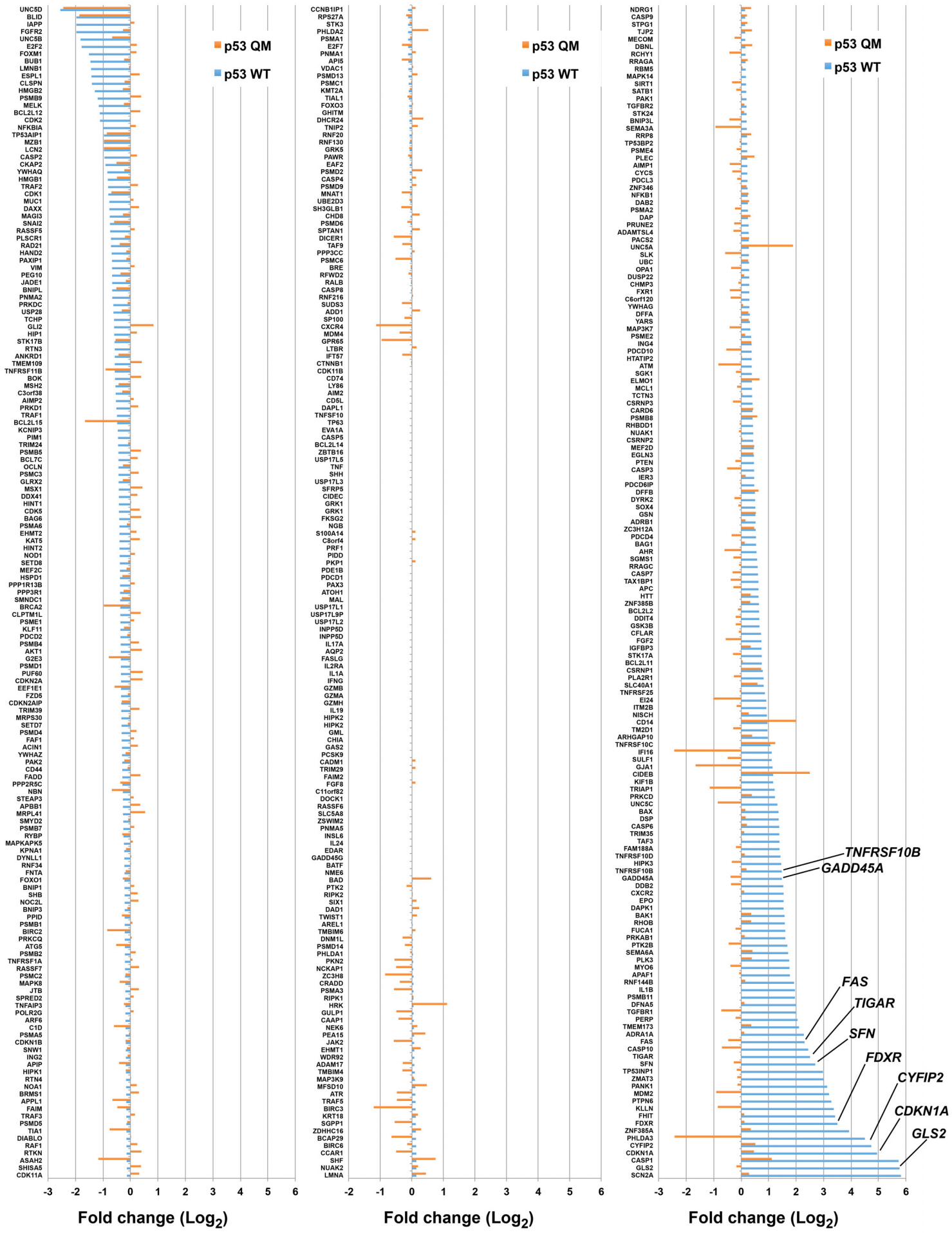

Figure S2_Oikawa

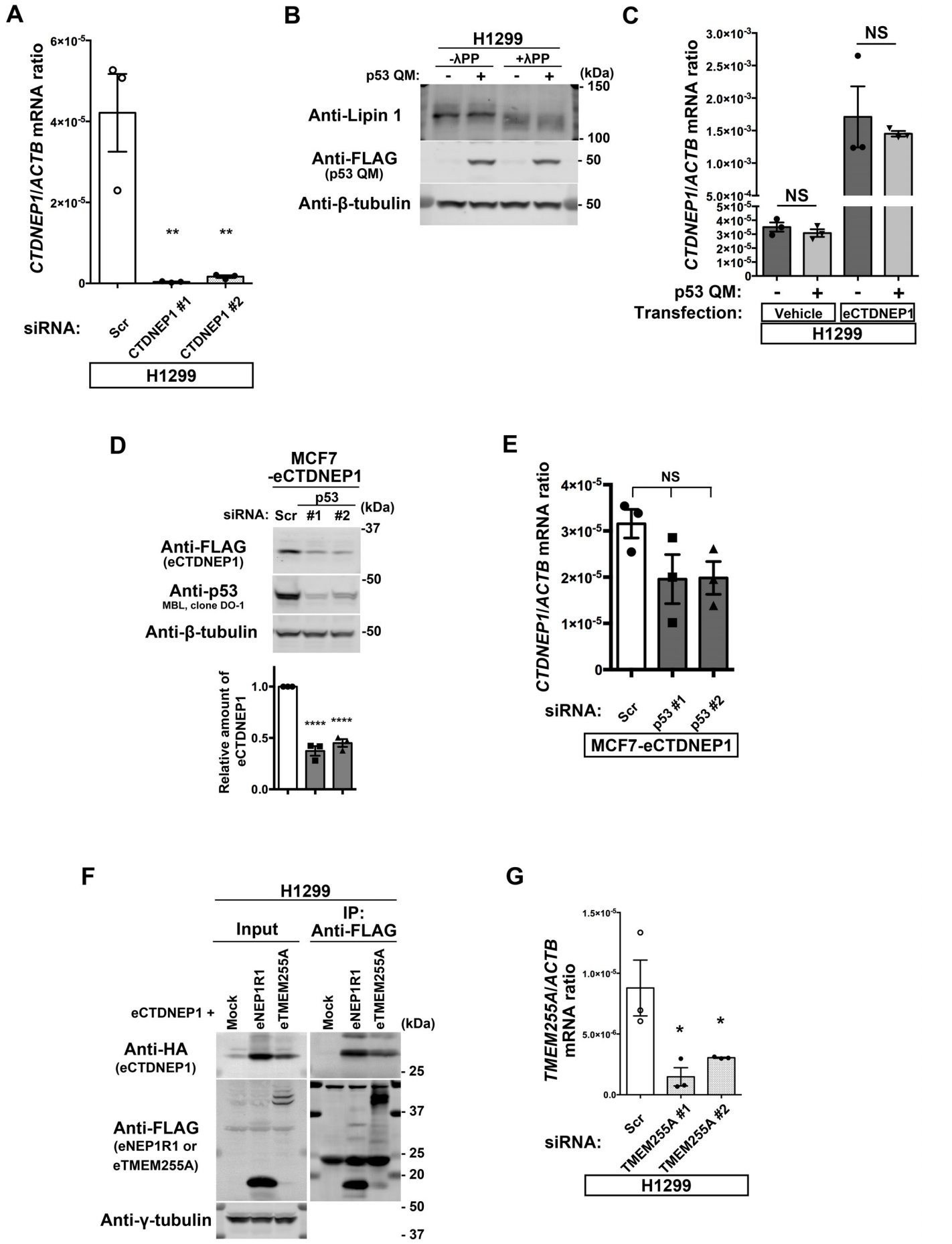

Figure S3_Oikawa